Valence-hole localization in core-valence doubly ionized states of ionic molecules and its impact on *KLV* Auger spectroscopy

H. D. Schulte and L. S. Cederbaum
Theoretische Chemie, Physikalisch-Chemisches Institut, Universität Heidelberg, 69120 Heidelberg, Germany

F. Tarantelli
Dipartimento di Chimica and Centro Studi CISM del CNR, Università di Perugia, I-06123 Perugia, Italy
(Received 25 January 1999; revised manuscript received 3 June 1999)

The complete spectra of core-valence dicationic states, i.e., states with one vacancy in the core and one in the valence shell, of the molecules BF_3, AlF_3, BCl_3, and $AlCl_3$, are investigated by the Green's-function method. An analysis of the double-hole density in the corresponding correlated states shows that when the core hole is on a ligand (halogen) atom, the valence hole is also strongly localized, either on the same ligand or on a different ligand. As a result these states can be classified as either *on-core* or *off-core site* states. We discuss how the localization phenomena are at the origin of the chlorine *KLV* Auger spectra of BCl_3 and $AlCl_3$ and, in particular, how they provide a complete and conclusive interpretation of these spectra. Due to the intra-atomic nature of the Auger process, the simulation of the chlorine and aluminum *KLV* Auger spectra is done by a simple convolution of the respective on-core site component of the computed two-hole density distribution. The ligand atom spectra contain almost no information about the molecular system, representing an indistinct *self-image* of the ligand atom itself, whereas the central atom spectra render a distinct *foreign image* of the molecular environment. [S1050-2947(99)07009-2]

PACS number(s): 31.25.−v, 32.80.Hd

I. INTRODUCTION

Auger spectra have been used extensively for sample analysis of elements and for surface structure analysis by means of so-called scanning Auger and surface imaging Auger techniques [1]. For molecules, the Auger experiment has mostly been used as a spectroscopic tool to obtain information on dicationic states. It is in this respect complementary to other experimental methods, for example double-charge-transfer spectroscopy [2], charge-stripping mass spectroscopy [3,4], and double coincidence experiments [5–8], namely, photoion-photoion, photoelectron-photoion or photoelectron-photoelectron experiments.

Three types of molecular Auger spectra can be distinguished: those spectra involving transitions between core shells only, those for which both final-state vacancies are distributed among valence molecular orbitals, and those spectra in which one of the final-state vacancies has valence character and the other one core character. The core-type spectra are rather straightforward to interpret since they essentially exhibit atomic character [9–12]. These spectra show an internal invariance with respect to energies and intensities, but respond to different ligand substitutions with small but uniform shifts, the Auger chemical shifts. The second kind of spectra, the molecular valence spectra [so-called core-valence-valence (CVV) spectra], are governed by nonradiative decay between initial, well-localized, core-hole states and final states with holes in the valence shell. They are the ones most commonly investigated experimentally [13–16] and theoretically [17–25].

The third kind of Auger spectra, for example *KLV* spectra of molecules containing second-row atoms, have rarely been investigated, both experimentally and theoretically. Generally speaking, there is a lack of investigations on molecular core-valence dicationic states. Recently, the present authors carried out a first systematic theoretical study on the core-valence double vacancies in CO, N_2, and H_2CO using Green's-function and configuration-interaction methods [26]. In that work the numerical results were analyzed in terms of perturbation theory and with the aid of a two-hole ($2h$) atomic population analysis measuring the extent of hole localization in the dicationic states.

For the generation of core-valence dicationic states of first-row molecules, various experimental techniques can be envisaged, in principle the most straightforward being the direct double ionization of one core electron and one valence electron. Indeed, the first experimental determination recently succeeded of an absolute double photoionization cross section for the direct emission into the continuum of $2p$ (core) and $3s$ (valence) electrons in sodium atoms [27]. Another possibility is to produce a primary vacancy in an inner atomic subshell (core). In this case the desired dicationic states can result from two different mechanisms. In a one-step mechanism a valence electron is simultaneously ejected due to relaxation effects in the valence shell. This is the so-called shake-off process accompanying core ionization [28]. Alternatively, in a two-step process, the dicationic states can be generated by *valence ionization out of an initially core-ionized system*. This case is interesting, since it allows one to view the resulting spectrum as a ''normal'' ionization spectrum in the presence of a well-defined core hole localized on a particular atom [26].

In the Auger process the ejection of the primary core electron is followed by decay of the singly charged ion, leading to the emission of a second electron and, thus, to the production of a doubly charged ion. In order to produce core-valence dicationic states via the Auger process the primary (deep) core hole has to be localized on an atom which con-

tains at least one more energetically higher shell which is still a core shell. If, for example, the primary core hole is localized in the K shell of a second row atom, the KLV Auger process produces final dicationic states with one L shell (core) and one valence vacancy. To date, such core-core-valence (CCV) Auger experiments are confined to rare gases [29,30] and solids [15,31], in the latter case especially to metals, alloys, and silicon. The Auger decay is a particularly interesting source for the production of core-valence dicationic states. Owing to its intra-atomic nature, it can roughly be thought of as a probe of the magnitude of the $2h$ density in the final dicationic states at the atomic site where the primary decaying core hole is created. It is clear that only states which have a significant relative component of the $2h$ density located at a given atom can have an appreciable rate of decay from the corresponding core hole [14,15,18,20–22].

In the present paper we discuss the results of *ab initio* Green's-function calculations on the various core-valence doubly ionized states of BF_3, AlF_3, BCl_3, and $AlCl_3$. These halogenides, especially the fluorides, can be expected to be particularly well-suited examples to study hole localization phenomena in the dicationic states, since they present ionic bonds and possess symmetry equivalent ligand atoms. In such systems the quasidegenerate ligand core orbitals are delocalized over the equivalent atoms and the corresponding symmetry-adapted core-valence dicationic states have to be represented in a configuration space containing all equivalent delocalized core levels. But it is possible to construct symmetry-reduced dicationic states in a configuration space containing only those localized core orbitals which are confined to one single atom. The dicationic states of the above molecules are automatically adapted to D_{3h} symmetry when the core hole is created on the central atom, but are reduced to C_{2v} symmetry when a localized core hole is created on a ligand atom. The validity and usefulness of this *localized core approximation* has been discussed [26,32–36] for the manifold of general core states comprising core ionized, core excited, core-valence dicationic states, etc., and found to be very satisfactory. Also the understanding of the very relevant hole-hole interaction in core-valence dicationic states is facilitated by the use of localized core orbitals. Since this interaction depends on the localization of the valence hole relative to the core hole, we are only left with the problem of the valence-hole distribution by confining each core orbital to its atomic space. Accordingly, our discussion will be done in the more transparent localized core picture. We shall discuss the extent to which hole localization takes place in the dicationic states of the above D_{3h} molecules, and how it affects the energy position and intensity in the aluminum and chlorine KLV Auger spectra.

II. COMPUTATIONAL DETAILS

The theoretical framework which was used to compute the core-valence dicationic states is based on a second-order approximation scheme for the two-particle Green's function known as the algebraic diagrammatic construction [ADC(2)] [37,38]. The formalism has already been discussed extensively in the literature in relation to the core [9,12] and, in particular, to valence doubly ionized states [20,23,39,40]. For a general overview of its implementation and application to Auger spectroscopy, see Refs. [24,25]. Here we briefly recall that the approximation scheme used for the particle-particle propagator leads to a Hermitian eigenvalue problem in the space of dicationic configurations of the system under consideration, built on the basis of the Hartree-Fock orbitals of the neutral system. The eigenvalues and eigenvectors can be directly related to the double ionization energies and to the residue amplitudes of the propagator, respectively. This approximation takes into account the $2h2p$ ground-state correlation as well as the $4h2p$ contributions for the $2h$ main states, while the explicit configuration space only comprises the dicationic $2h$ and $3h1p$ configurations (defined in the basis of the neutral ground-state Hartree-Fock orbitals). The resulting eigenvalues give size-consistent ionization energies which are correct beyond second order for *main states* (i.e., states perturbatively derived from the $2h$ space) and beyond first order for *satellite states* (derived from $3h1p$ configurations).

Using ADC(2), we computed the core-valence double-ionization potential (DIP_{cv}) and the pole strength distribution of the F $1s$, B $1s$, Cl $2s$ and $2p$, and Al $2s$ and $2p$ valence dicationic states of the appropriate molecules. Here and in the following, the term ''F $1s$ valence,'' for example, means one vacancy in the $1s$ core of fluorine and another vacancy in the valence shell. In principle, these states could be calculated with the complete ADC(2) scheme described above. However, only in a quite inefficient manner, since the eigenvalues of the ADC matrices are calculated from the edge of the spectrum but the dicationic states with one core vacancy and one valence vacancy are rather situated in its central part. By adopting a core-valence separation approximation [35], on the other hand, these states can be computed directly, independent of those states with two core or two valence vacancies. In core-valence separation the ADC(2) space is restricted to those $2h$ and $3h1p$ configurations with *exactly one* core hole. Hereby the ADC matrix dimension is considerably reduced. In order to assess the inaccuracy introduced by the core-valence separation, we will discuss the F $1s$ valence dicationic states of BF_3 in Sec. III D, calculated both in core-valence separation and with the complete ADC(2).

In the outermost part of the core-valence spectra, the density of dicationic states is low and, except for the $2h$ configuration mixing often required to describe hole localization effects, the independent particle picture of ionization remains largely valid (albeit in a localized orbital model). By contrast, in the inner parts of the spectra and, in particular, when the core hole results from the Al $2s$ or Cl $2s$ orbitals, breakdown effects of the orbital picture of ionization [41] may occur, leading to a large number of states with small $2h$ weight, and areas with a high density of states. To calculate the eigenvalues for such dense inner parts of the spectra, we employed a recently implemented block-Lanczos procedure [25] using as seed the main space of $2h$ configurations. With this technique one accurately computes, rather than individual eigensolutions, the *envelope* of the dense pole strength distribution which, as will be discussed, can be related to the Auger spectrum. It can be shown [42] that the block-Lanczos procedure provides a convergence rate on the spectrum of main space components which is exponential in the width of the lines making up the spectrum. In the present case, with

an assumed width of 1.5 eV, convergence on the Al $2s$ and Cl $2s$ spectra was obtained after 300 block-Lanczos iterations. The states in the B $1s$, F $1s$, Al $2p$, and Cl $2p$ spectra were also *individually* converged.

The calculations for all molecules have been carried out in a triple-ζ basis set [43] consisting of $5s$ and $3p$ contracted Cartesian Gaussians on the first-row elements and $6s$ and $5p$ on the second-row elements, always enlarged by one polarization function on each atom with an exponent of 0.5 for B, 1.62 for F, 0.311 for Al, and 0.619 for Cl [44]. The experimental bond lengths for B-F, Al-F, B-Cl, and Al-Cl of 1.295, 1.63, 1.74, and 2.06 Å, respectively, have been used [45]. In the ADC calculations on BCl_3 ($AlCl_3$) the 16 (20) highlying corelike virtual orbitals have been excluded from the configuration space. Moreover, the ADC computations on the F $1s$ and Cl $2s$ and $2p$ valence dicationic states are based on the localized core approximation. The calculation of the symmetry-reduced states in the localized core representation is done by including only one atomic set of localized F $1s$ or Cl $2s$ and $2p$ orbitals in the active ADC configuration space. As a result of the atomic localization of the core orbitals (carried out by the Foster-Boys transformation), the system X^*MX_2—the molecule with one ligand core hole—does not possess full D_{3h} symmetry but C_{2v} symmetry. The valence orbitals are not affected by this transformation and maintain their D_{3h} symmetry also in the localized core representation. In the case of BF_3 we have computed both its symmetry-adapted and symmetry-reduced F1s valence dicationic states. The quasidegeneracy of the symmetry-adapted states was found to be reflected by the energy gap of only few meV, and the almost identical $2h$ weight and state composition for each state pair (each pair formed by one state of A symmetry and one of E symmetry). Thus, the localized core representation turns out to be an excellent approach, since the computed DIP_{cv}, $2h$ weight, and composition of each symmetry-reduced state is approximately given by the respective mean value for the quasidegenerate (A,E) pair.

III. F 1s VALENCE DICATIONIC STATES OF BF_3 AND AlF_3

A. Dicationic states and double ionization energies of BF_3

For an ionic molecule like BF_3, one expects the valence electron density to be mainly located on the electronegative constituents. The neutral ground state of the system can be visualized by a valence bond model with an ionic σ bond between the boron and each fluorine atom, and three nonbonding lone pairs concentrated around each fluorine. The HF ground-state configuration of BF_3 (D_{3h} symmetry) is

$$(\text{core})(1a_1')^2(1e')^4(2a_1')^2(2e')^4(1a_2'')^2 \times(3e')^4(1e'')^4(1a_2')^2.$$

An interpretation of the molecular orbitals can be obtained by a Mulliken population analysis. F $1s$ orbitals of a_1' and e' symmetry differ by less than 1 meV from each other and have an identical population. The valence shell can be subdivided into two regions: the inner valence $(1a_1',1e')$ and the outer valence, which are mainly of of fluorine $2s$ and $2p$ character, respectively. The ionic sp^2 bonding is exercised mostly through the outer valence orbitals $2a_1'$ and $2e'$, but also the out-of-plane orbital $1a_2''$ has some bonding character. The remaining three outermost orbitals $3e'$, $1e''$, and $1a_2'$ represent almost pure fluorine lone pairs.

The double ionization energy (DIP_{cv}) and $2h$ composition of the localized F $1s$ valence dicationic states of BF_3, calculated with the ADC(2) scheme in core-valence separation, are reported in Table I. We shall often simply use the term ''energy'' to refer to the binding energy of the two electrons, i.e., DIP_{cv}, rather than to the total energy of the dicationic states. According to the number of inner and outer valence orbitals and the large energy gap between them one finds 12 singlet states and 12 triplet main states which can be separated into two principal groups: one group, between 717.8 and 739.5 eV, comprises nine singlet states and nine triplet states with an outer valence hole; a second group above 743.0 eV is made up of three singlets and three triplets having an inner valence hole (in the latter region some satellite states also appear, on which we shall comment in Sec. III C). As is evident in Table I, each of these two groups can itself be divided on energy grounds into two subgroups (separated by horizontal lines in the table): in the outer valence region there are six singlet states and six triplet states between 717.8 and 722.6 eV, and three states of each spin between 734.2 and 739.5 eV; in the inner valence region one finds two states of each multiplicity in the range 743.0–743.9 eV and finally two main states $^3A_1$ and $^1A_1$ at 757.8 and 763.7 eV, respectively. Consequently, there are four evident groups of F $1s$ valence dicationic states of BF_3. As will be explained in Sec. III B, this grouping and the relative energy of singlet and triplet states are uniquely determined by the localized character of the two-hole density distribution. The evident configuration mixing seen in Table I for all dicationic states, except some of A_2 (B_2) symmetry in the outer (inner) valence region, will be seen to be the mechanism for hole localization.

B. Two-hole population analysis and atomic localization of the valence hole

To determine the distribution and the extent of localization of the valence hole in core-valence dicationic states, we have used a correlated two-hole density population analysis of the dicationic states [20]. By this analysis the total $2h$ weight of an ADC eigenvector is decomposed into its localized atomic contributions. The sum of the contributions of the atomic orbital hole pairs p and q to the $2h$ weight, where both p and q refer to basis functions centered on a given atom X, is the *one-site* contribution of that atom, and measures the extent to which both holes in the dicationic state are localized on atom X. Similarly, the *two-site* character of a state is measured by the sum of terms p and q which refer to basis functions centered on two different atoms X and Y. Thus the predominance of one of these contributions for a given state indicates that the two vacancies are strongly localized in space (either at the same or each at another atomic center), whereas states for which more than one component is significantly present are characterized as having correspondingly delocalized holes.

TABLE I. Computed double-ionization potential (DIP_{cv}) and composition of the F 1*s* valence dicationic states of BF_3. In order to compute the core-valence dicationic states directly, the calculations were done with the ADC(2) scheme in core-valence separation (see Sec. II). Each state is labeled in the reduced C_{2v} symmetry in the localized core representation, and corresponds to three quasidegenerate states of D_{3h} symmetry in the delocalized core representation. The composition reported is given by the square $2h$ components of the ADC eigenvectors with a $2h$ weight larger than 0.01. The $2h$ configurations are indicated by the occupied orbital of BF_3 from which the valence electron is removed.

Character	State	DIP_{cv} (eV)	$2h$ weight	$2h$ composition
Outer valence	$^3B_2$	717.8042	0.7864	$0.5028(1a_2')0.2789(3e_x')0.0048(2e_x')$
off-core site	$^1B_2$	717.8044	0.7864	$0.4958(1a_2')0.2856(3e_x')0.0050(2e_x')$
	$^1A_2$	718.2244	0.7865	$0.7865(1e_x'')$
	$^3A_2$	718.2316	0.7866	$0.7866(1e_x'')$
	$^3A_1$	719.3654	0.7861	$0.6469(3e_y')$ $0.1153(2e_y')0.0228(2a_1')0.0011(1e_y')$
	$^1A_1$	719.4137	0.7865	$0.6362(3e_y')0.1248(2e_y')0.0239(2a_1')0.0016(1e_y')$
	$^3B_1$	719.9436	0.7872	$0.4971(1a_2'')0.2900(1e_y'')$
	$^1B_1$	719.9634	0.7874	$0.5110(1a_2'')0.2764(1e_y'')$
	$^3B_2$	721.3257	0.7860	$0.5670(2e_x')0.1645(3e_x')0.0519(1a_2')0.0026(1e_x')$
	$^1B_2$	721.3553	0.7861	$0.5850(2e_x')0.1512(3e_x')0.0473(1a_2')0.0026(1e_x')$
	$^3A_1$	722.5507	0.7861	$0.4687(2a_1')0.3046(2e_y')0.0106(3e_y')0.0013(1e_y')$
	$^1A_1$	722.5587	0.7861	$0.4777(2a_1')0.2951(2e_y')0.0111(3e_y')0.0016(1e_y')$
Outer valence	$^3B_1$	734.2457	0.7398	$0.4644(1e_y'')0.2754(1a_2'')$
on-core site	$^3B_2$	734.3523	0.7375	$0.3206(3e_x')0.2139(1a_2')0.2001(2e_x')0.0029(1e_x')$
	$^3A_1$	736.4120	0.7403	$0.3445(2e_y')0.2741(2a_1')0.1185(3e_y')0.0016(1e_y')0.0015(1a_1')$
	$^1B_1$	737.4946	0.7451	$0.4829(1e_y'')0.2622(1a_2'')$
	$^1B_2$	737.6207	0.7416	$0.3283(3e_x')0.2265(1a_2')0.1792(2e_x')0.0076(1e_x')$
	$^1A_1$	739.5022	0.7459	$0.3438(2e_y')0.2587(2a_1')0.1314(3e_y')0.0086(1e_y')0.0034(1a_1')$
Inner valence	$^3B_2$	743.0409	0.7756	$0.7705(1e_x')0.0049(2e_x')$
off-core site	$^1B_2$	743.0570	0.7754	$0.7659(1e_x')0.0073(2e_x')0.0011(3e_x')0.0011(1a_2')$
	$^3A_1$	743.8705	0.7746	$0.4913(1a_1')0.2779(1e_y')0.0050(2a_1')$
	$^1A_1$	743.9102	0.7746	$0.5032(1a_1')0.2592(1e_y')0.0096(2a_1')0.0024(2e_y')$
Inner valence	$^3A_1$	757.8519	0.6466	$0.4139(1e_y')0.2322(1a_1')$
on-core site	$^3A_1$	757.9040	0.0485	$0.0284(1e_y')0.0201(1a_1')$
	$^3A_1$	757.9465	0.0321	$0.0185(1e_y')0.0130(1a_1')$
	$^1A_1$	763.7328	0.7041	$0.4574(1e_y')0.2439(1a_1')0.0016(2a_1')$

Since the core hole is localized on a specific atom, only the problem of the valence-hole distribution remains to be analyzed in the case of core-valence dicationic states. If the core vacancy is localized on atom *X*, we can separate the $2h$ population of each ADC eigenvector in one *on-core site* contribution *X* (the valence hole on the atom which carries the core hole) and *off-core site* contributions *Y* (the valence hole on a different atom), while other contributions vanish. Thus, for example, in the case of F^*BF_2—the molecule with a core vacancy localized on one fluorine atom—we can separate the total $2h$ weight of the ADC states in the on-core site contribution F* and the two off-core site contributions F and B.

The results of the $2h$ population analysis of the F 1*s* valence dicationic states of BF_3, reported in Table II, give a simple and unambiguous explanation for the observed grouping of the states. All states are dominated either by the fluorine *on-core site* (F*) or by the fluorine *off-core site* (F) component. The boron off-core site (B) contribution increases toward the end of the first group of outer valence off-core site states because of the greater bonding character of the $1a_2''$, $2e'$, and $2a_1'$ orbitals, but remains very small throughout the spectrum. By this very pronounced localization of the valence vacancy at the fluorine sites, the electrostatic hole-hole repulsion is minimized in the off-core site states and maximized in the on-core site states. This determines the energy and the singlet-triplet splitting of the dicationic states. States with smaller binding energy in the inner and outer valence regions are off-core site states, while those with larger energy are on-core site states. In the ideal case of perfect localization of the core and valence holes at different fluorine atoms, the singlet-triplet splitting would be zero; it is in reality a very small value less than 0.05 eV. Conversely, the singlet-triplet splitting is remarkably large for the on-core site states, and there is a significant difference (3.2 eV vs. 5.9 eV) between the values in the outer and inner valence regions. This is easily explained by the higher charge density of the inner valence orbitals and, in addition, by the fact that the interaction between the core hole and the outer valence hole is screened by the inner valence electrons.

How does valence-hole localization take place in the dicationic states? The state composition in Table I explains the valence-hole localization mechanism in the delocalized symmetry-adapted valence representation. The localization of the valence hole is realized by the mixing of $2h$ configu-

TABLE II. Double-ionization potential (DIP_{cv}) and two-hole atomic population analysis of the ADC $2h$ weights for the F1s valence dicationic states of BF_3. F* denotes the fluorine atom that carries the localized core hole, and the $2h$ population columns are labeled by the atom where the valence hole is localized.

			$2h$ population			total
Character	State	DIP_{cv} (eV)	F*	F	B	$2h$ weight
Outer valence	$^3B_2$	717.8042	−0.0000	0.7721	0.0144	0.7864
off-core site	$^1B_2$	717.8044	−0.0004	0.7721	0.0147	0.7864
	$^1A_2$	718.2244	0.0000	0.7665	0.0200	0.7865
	$^3A_2$	718.2316	0.0000	0.7667	0.0200	0.7866
	$^3A_1$	719.3654	0.0017	0.7454	0.0391	0.7861
	$^1A_1$	719.4137	−0.0001	0.7468	0.0398	0.7865
	$^3B_1$	719.9436	0.0008	0.7083	0.0780	0.7872
	$^1B_1$	719.9634	−0.0007	0.7084	0.0796	0.7874
	$^3B_2$	721.3257	0.0049	0.6765	0.1046	0.7860
	$^1B_2$	721.3553	0.0019	0.6784	0.1058	0.7861
	$^3A_1$	722.5507	0.0001	0.6700	0.1160	0.7861
	$^1A_1$	722.5587	−0.0003	0.6705	0.1160	0.7861
Outer valence	$^3B_1$	734.2457	0.6911	−0.0022	0.0509	0.7398
on-core site	$^3B_2$	734.3523	0.6988	0.0098	0.0288	0.7375
	$^3A_1$	736.4120	0.6137	0.0081	0.1184	0.7403
	$^1B_1$	737.4946	0.6978	−0.0022	0.0495	0.7451
	$^1B_2$	737.6207	0.6999	0.0153	0.0264	0.7416
	$^1A_1$	739.5022	0.6048	0.0164	0.1247	0.7459
Inner valence	$^3B_2$	743.0409	0.0055	0.6818	0.0883	0.7756
off-core site	$^1B_2$	743.0570	0.0119	0.6743	0.0891	0.7754
	$^3A_1$	743.8705	0.0072	0.6753	0.0921	0.7746
	$^1A_1$	743.9102	0.0149	0.6664	0.0934	0.7746
Inner valence	$^3A_1$	757.8519	0.5836	0.0003	0.0628	0.6466
on-core site	$^3A_1$	757.9040	0.0435	0.0003	0.0047	0.0485
	$^3A_1$	757.9465	0.0285	0.0005	0.0031	0.0321
	$^1A_1$	763.7328	0.6434	−0.0004	0.0611	0.7041

rations. Let us consider A_2 and B_1 states which derive from the out-of-plane valence orbitals $1a_2''$ and $1e''$. The $1e_x''$ component alone may contribute to the symmetry-reduced A_2 states. Since the valence orbital $1e_x''$ is exclusively delocalized over the two fluorine atoms which do not carry the core vacancy, the A_2 states are automatically *off-core site* states. In contrast to this, the B_1 states require the $2h$ mixing of $1e_y''$ and $1a_2''$ in order to localize the valence hole in the corresponding off-core site and on-core site states, because the valence orbitals $1e_y''$ and $1a_2''$ are delocalized over all three fluorine atoms. Similar arguments hold for the inner valence A_1 and B_2 states which derive from the orbitals $1a_1'$ and $1e'$.

C. Similarities in the dicationic states of BF_3 and AlF_3

Valence-hole localization in the core-valence dicationic states is a completely general phenomenon for molecules like the ones studied here, which possess strongly electronegative, symmetry-equivalent ligands which carry the core hole. This is illustrated by comparing the F 1s valence dicationic states of BF_3 and AlF_3. For this purpose, here we avoid presenting the complete lengthy tables of dicationic states for AlF_3, and the following summary will suffice. Both molecules have the same HF valence configuration and a similar population of the corresponding orbitals. We obtain a spectrum of correlated dicationic main states of AlF_3 which is very much like that of BF_3, both in $2h$ composition and $2h$ population of the states. The complete spectrum of AlF_3 is made up of the same sequence of main states as the BF_3 one, except that, at the high-energy end, one satellite state accompanying the $^1A_1$ inner valence on-core site main state is found instead of the two satellites of the $^3A_1$ main state in the BF_3 spectrum. Our data on AlF_3 equivalent to Tables I and II for BF_3 can be obtained upon request.

The results of the $2h$ population analysis for the F 1s valence dicationic states of BF_3 and AlF_3 are summarized in Table III and visualized in Fig. 1. They demonstrate very clearly that the same clearcut localization of the valence hole takes place in the dicationic states of BF_3 and AlF_3, leading to an equal grouping of states in the spectra of both molecules. In Fig. 1 we show the separate spectra of F* (full area) and F (striped area) components to the total $2h$ weight, convoluted with a FWHM (full width at half maximum) of 1.5 eV. This illustrates how the states cluster in four distinct groups, two of which (labeled B and D) are further split into two subgroups of singlet and triplet states. It also makes evident the alternating pattern of the F and F* character as

TABLE III. Average two-hole population and variance in percent of the total $2h$ weight for the six groups of F $1s$ valence dicationic states of BF_3 and AlF_3. The labeling of the peaks refers to Fig. 1.

	BF_3			AlF_3		
Peak	F*	F	B	F*	F	Al
A	0.08 ± 0.19	91.99 ± 5.16	7.92 ± 5.08	-0.01 ± 0.04	94.02 ± 3.36	5.99 ± 3.35
B_1	90.36 ± 5.30	0.71 ± 0.72	8.93 ± 5.14	93.65 ± 3.64	0.08 ± 0.14	6.27 ± 3.51
B_2	89.70 ± 6.10	1.32 ± 1.14	8.98 ± 5.62	93.35 ± 4.04	0.31 ± 0.41	6.34 ± 3.64
C	1.27 ± 0.48	87.02 ± 0.67	11.70 ± 0.27	0.25 ± 0.24	93.38 ± 0.54	6.36 ± 0.33
D_1	89.57 ± 0.57	0.70 ± 0.58	9.73 ± 0.05	94.45 ± 0.00	-0.01 ± 0.00	5.56 ± 0.00
D_2	91.38 ± 0.00	-0.06 ± 0.00	8.67 ± 0.00	94.81 ± 0.09	0.03 ± 0.05	5.15 ± 0.04

well as the complete dominance of one or the other component. The small difference between the sum of the fluorine contributions and the total $2h$ curve is due to the central atom (B or Al) component. These findings are fully confirmed by the average $2h$ population of the six peaks in Table III. The even more pronounced valence-hole localization in the dicationic states of AlF_3 reflects the more ionic character of this molecule. Here one finds a rather constant contribution of the F or F* component to the total $2h$ weight of about 94%, whereas it varies from 87 to 92% for BF_3.

With the aid of Table III and Fig. 1, we can now analyze the various groups of dicationic states in more detail. The first group (labeled A) is made up of outer valence off-core site states. The large charge separation minimizes the Coulomb repulsion between the core and valence holes as well as their exchange interaction. Accordingly, group A is found at the low-energy side of the spectra, and singlet-triplet pairs of states are close in energy, separated by less than 0.05 eV. Despite their common characterization, peaks A in Fig. 1 exhibit two obvious differences due to the stronger off-core site localization in the dicationic states of AlF_3 compared to BF_3. First, the onset of the AlF_3 spectrum is at lower energy (713.7 eV for AlF_3 and 717.8 eV for BF_3). This is partly due to the smaller orbital energies, and partly to the smaller hole-hole repulsion in AlF_3 because of the larger Al-F distance. Second, peak A in the AlF_3 spectrum is narrower. The latter finding is a consequence of the smaller energy range covered by the outer valence electrons of AlF_3 (2.9 eV vs 5.5 eV for BF_3), and is immediately understood by considering that, in comparison to BF_3 with its ionic sp^2 bonding, AlF_3 can be almost imagined as a strongly ionic system with four nonbonding lone pairs around each fluorine atom.

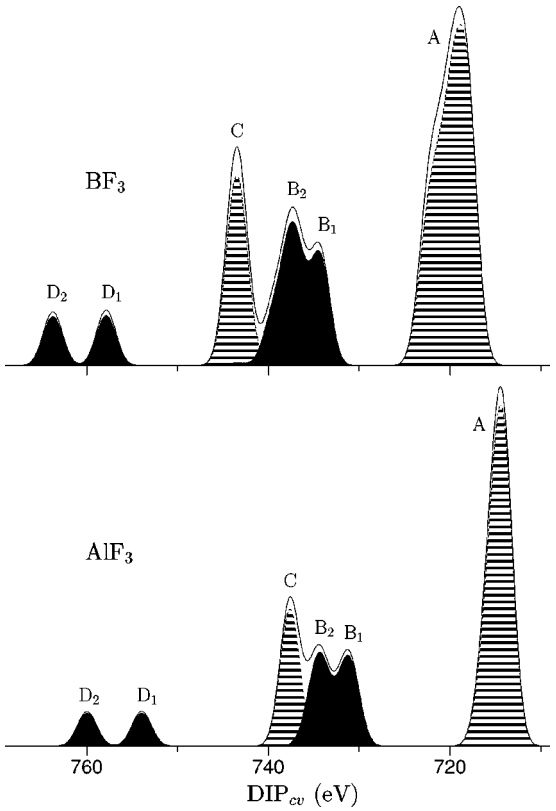

FIG. 1. Full curves represent the Gaussian convolution (FWHM 1.5 eV) of the total ADC $2h$ weight of the F $1s$ valence dicationic states of BF_3 and AlF_3. The striped areas visualize the off-core site F component and the full areas reflect the on-core site F* component of the $2h$ weight. The remaining area is due to the off-core site central atom component.

Group A is followed by its on-core site counterpart B, comprising states with the outer valence hole confined to the F* atom carrying the core hole. The highest lying state of group A and the lowest-lying state of group B are separated by a gap of 11.7 and 14.8 eV for BF_3 and AlF_3, respectively, owing to the broader energy range covered by peak A in the case of BF_3. The data show that the states of group B actually split into two distinct subgroups B_1 and B_2 which, comprise the triplet and singlet states, respectively. The asymmetry of peak B in the BF_3 spectrum is due to the fact that the highest-lying triplet state is closer in energy to the lowest singlets than to the other triplets (see Table I), whereas singlet and triplet states are well separated by more than 2 eV in the case of AlF_3. The splitting for each singlet-triplet pair within group B is about 3.2 eV and can easily be understood in view of the strong localization of both positive charges on the same atom.

In the next group (labeled C) the states are characterized as having the valence hole in the inner valence shell of one F atom (different from the F* atom). Again the singlet-triplet splitting within this group of off-core site states is less than 0.05 eV. The energy gap between the lowest lying state of group C and the highest-lying state of B_2 is 3.5 eV and 2.3 eV for BF_3 and AlF_3, respectively. The inner valence off-core site states are followed by their triplet (D_1) and singlet (D_2) on-core site counterparts. The latter two groups are widely separated in energy (by about 6 eV) due to the local-

TABLE IV. Computed double-ionization potential (DIP_{cv}) and composition of the F 1*s* valence dicationic states of BF_3. The calculations were done with the full ADC(2) scheme for the computation of generic dicationic states (see Sec. II). Δ is the deviation of the given DIP_{cv} from the corresponding value in core-valence separation reported in Table I. For other details, see the caption of Table I.

Character	State	DIP_{cv} (eV)	Δ (eV)	$2h$ weight	$2h$ composition
Outer valence	$^3B_2$	717.3823	0.4219	0.7886	$0.5041(1a_2')0.2798(3e_x')0.0048(2e_x')$
off-core site	$^1B_2$	717.3827	0.4217	0.7886	$0.4973(1a_2')0.2863(3e_x')0.0050(2e_x')$
	$^1A_2$	717.8028	0.4216	0.7887	$0.7887(1e_x'')$
	$^3A_2$	717.8098	0.4218	0.7889	$0.7889(1e_x'')$
	$^3A_1$	718.9436	0.4218	0.7884	$0.6487(3e_y')0.1156(2e_y')0.0229(2a_1')0.0011(1e_y')$
	$^1A_1$	718.9905	0.4232	0.7887	$0.6382(3e_y')0.1250(2e_y')0.0240(2a_1')0.0016(1e_y')$
	$^3B_1$	719.5215	0.4221	0.7894	$0.4986(1a_2'')0.2908(1e_y'')$
	$^1B_1$	719.5408	0.4225	0.7896	$0.5121(1a_2'')0.2775(1e_y'')$
	$^3B_2$	720.9042	0.4215	0.7882	$0.5687(2e_x')0.1649(3e_x')0.0520(1a_2')0.0026(1e_x')$
	$^1B_2$	720.9332	0.4221	0.7883	$0.5864(2e_x')0.1518(3e_x')0.0476(1a_2')0.0026(1e_x')$
	$^3A_1$	722.1291	0.4216	0.7883	$0.4701(2a_1')0.3055(2e_y')0.0106(3e_y')0.0013(1e_y')$
	$^1A_1$	722.1368	0.4219	0.7884	$0.4789(2a_1')0.2961(2e_y')0.0111(3e_y')0.0016(1e_y')$
Outer valence	$^3B_1$	733.8523	0.3934	0.7420	$0.4659(1e_y'')0.2761(1a_2'')$
on-core site	$^3B_2$	733.9600	0.3923	0.7397	$0.3216(3e_x')0.2146(1a_2')0.2005(2e_x')0.0029(1e_x')$
	$^3A_1$	736.0153	0.3967	0.7425	$0.3456(2e_y')0.2748(2a_1')0.1189(3e_y')0.0016(1e_y')0.0015(1a_1')$
	$^1B_1$	737.0218	0.4728	0.7476	$0.4842(1e_y'')0.2634(1a_2'')$
	$^1B_2$	737.1477	0.4730	0.7442	$0.3293(3e_x')0.2271(1a_2')0.1802(2e_x')0.0075(1e_x')$
	$^1A_1$	739.0307	0.4715	0.7483	$0.3452(2e_y')0.2600(2a_1')0.1316(3e_y')0.0082(1e_y')0.0034(1a_1')$
Inner valence	$^3B_2$	742.6237	0.4172	0.7781	$0.7729(1e_x')0.0049(2e_x')$
off-core site	$^1B_2$	742.6394	0.4176	0.7779	$0.7684(1e_x')0.0072(2e_x')0.0011(3e_x')0.0011(1a_2')$
	$^3A_1$	743.4537	0.4168	0.7772	$0.4929(1a_1')0.2789(1e_y')0.0051(2a_1')$
	$^1A_1$	743.4917	0.4185	0.7772	$0.5042(1a_1')0.2610(1e_y')0.0095(2a_1')0.0023(2e_y')$
Inner valence	$^3A_1$	757.4091		0.0328	$0.0188(1e_y')0.0138(1a_1')$
on-core site	$^3A_1$	757.4285	0.4234	0.6918	$0.4416(1e_y')0.2497(1a_1')$
	$^1A_1$	762.8355		0.0439	$0.0276(1e_y')0.0158(1a_1')$
	$^1A_1$	762.9603	0.7725	0.6810	$0.4430(1e_y')0.2347(1a_1')0.0019(2a_1')0.0004(F1s)$

ization of the inner valence hole on the core ionized atom.

Although we calculated all dicationic states with a $2h$ weight larger than 0.01 by ADC(2), there are exclusively main states with large $2h$ weight contributing to the groups *A*, *B*, and *C* of the BF_3 and AlF_3 spectra. Once valence-hole localization effects via $2h$ mixing are accounted for, these states can be interpreted within an independent-particle picture. But in the inner valence on-core site region (*D*) we encounter the situation that main states pass some of their $2h$ weight to accompanying satellites. This happens especially (see Table I) for the $^3A_1$ and $^1A_1$ inner valence on-core site states of BF_3 and AlF_3, respectively, and is an indication for a possible breakdown of the molecular orbital (MO) picture of ionization [41]. We emphasize, however, that the results obtained by ADC(2) for satellite states and energy regions where the breakdown of the MO picture of ionization may take place, have to be taken with care because only main states are consistently described beyond second order of perturbation theory by ADC(2). Breakdown regions are less accurately treated and a very high precision is needed to accurately compute them because of the quasidegeneracy of many electronic configurations in these energy ranges [26,41].

D. Influence of core-valence approximation on numerical results

In order to ascertain the impact of the core-valence approximation on the results, we have computed the F 1*s* valence dicationic states of BF_3 also with the full ADC(2) scheme (see Sec. II). The results of these calculations are given in Table IV. Both types of ADC calculations, with and without core-valence separation, have been performed in the reduced C_{2v} symmetry of the localized core representation. While the dimension of the ADC matrices, depending on space-spin symmetry, ranges from 10 790 to 17 228 without core-valence separation, it is only between 2019 and 3733 with core-valence separation. Although the full ADC(2) space comprises all $2h$ and $3h1p$ configurations which can be constructed from one localized F 1*s* orbital and the valence orbitals of BF_3, exclusively $2h$ and $3h1p$ configurations with exactly one core hole dominate the dicationic states. The most obvious $2h$ configuration not reflecting the core-valence separability of the dicationic states is the core-core double-hole configuration (F 1*s*). Its by far largest contribution (a square coefficient of 0.0004) is to the $^1A_1$ on-core site innermost valence state (see the last number in

TABLE V. Computed double-ionization potential (DIP_{cv}) and composition of the $^1A_1$ F $1s$ valence dicationic states of BF_3. The calculations were done with the ADC(2) scheme in extended core-valence separation (see Sec. III D). Δ is the deviation of the given DIP_{cv} from the corresponding value without core-valence separation reported in Table IV. For other details, see the caption of Table I.

Character	DIP_{cv} (eV)	Δ (eV)	$2h$ weight	$2h$ composition
Outer valence	719.4133	0.4228	0.7865	$0.6362(3e_y')0.1248(2e_y')0.0239(2a_1')0.0016(1e_y')$
off-core site	722.5586	0.4218	0.7861	$0.4777(2a_1')0.2951(2e_y')0.0110(3e_y')0.0016(1e_y')$
Outer valence on-core site	739.4904	0.4597	0.7459	$0.3440(2e_y')0.2589(2a_1')0.1314(3e_y')0.0082(1e_y')0.0035(1a_1')$
Inner valence off-core site	743.9090	0.4173	0.7746	$0.5025(1a_1')0.2601(1e_y')0.0095(2a_1')0.0024(2e_y')$
Inner valence	763.3489		0.0642	$0.0428(1e_y')0.0211(1a_1')$
on-core site	763.3739	0.4136	0.6487	$0.4211(1e_y')0.2247(1a_1')0.0017(2a_1')0.0004(F1s)$

Table IV). All other configurations discarded in core-valence separation enter the dicationic states with square coefficients smaller than 0.0001.

The comparison of the results obtained with and without core-valence separation shows that all but the inner valence on-core site states are described to a very good approximation within the core-valence separation. The $2h$ composition and the $2h$ weight of the dicationic main states are in good agreement and the difference Δ between the double ionization potentials (see Table IV) is approximately a constant value of ~ 0.4 eV. For the inner valence on-core site states, however, the inaccuracies introduced by core-valence separation are more pronounced. In the full ADC(2) scheme both the $^3A_1$ and $^1A_1$ main state pass some $2h$ weight to accompanying satellites, whereas only the $^3A_1$ main state does it in core-valence separation. As already mentioned, these findings for the satellites have to be taken with caution because they are less accurately treated in the ADC calculations (see Sec. III C). For the $^3A_1$ main state one finds as before $\Delta \simeq 0.4$ eV, but its leading $2h$ components $(1e_y')$ and $(1a_1')$ show larger deviations, with the consequence that the $2h$ weight of the $^3A_1$ main state in core-valence separation is smaller. In the case of the $^1A_1$ main state even the approximate constancy of Δ, found in all other cases, is violated. One finds $\Delta = 0.77$ eV and the $2h$ weight of the $^1A_1$ main state in core-valence separation is larger than the value obtained without core-valence separation. It thus appears that the $2h$ configuration (F $1s$), which is absent in core-valence separation, despite its small square coefficient of 0.0004, significantly affects the results for the $^1A_1$ inner valence on-core site state. It is evident that (F $1s$) may contribute considerably only to an inner valence on-core site state due to the direct interaction between the core hole and the inner valence hole localized on the same atom. In the localized core representation only this $2h$ configuration with two core holes is present and, in the reduced symmetry of F^*BF_2, it can influence only totally symmetric singlet states.

In order to take into account the influence of the core-core configuration (F $1s$) on the totally symmetric singlet states without otherwise renouncing to the advantages of the core-valence separation scheme, we have enlarged the $2h$ space by this single configuration and calculated the resulting additional interactions in the $2h$ space through first order. The results of this extended core-valence approximation are given in Table V. The comparison with the corresponding $^1A_1$ states in strict core-valence separation in Table I demonstrates that (F $1s$) acts appreciably only on the inner valence on-core site state as expected. The comparison with the full ADC(2) calculations in Table IV shows that the extended core-valence approximation reproduces roughly the on-core site inner valence main state and its accompanying satellite. Now the $2h$ weight of the $^1A_1$ main state lies 0.032 below the value without core-valence separation, and one finds $\Delta \simeq 0.4$ eV as for all other dicationic main states.

IV. Cl $2s$ AND $2p$ VALENCE DICATIONIC STATES OF BCl_3 AND $AlCl_3$

A. Results and analysis

The SCF results show that all four molecules here studied are described by the same HF valence configuration. In accord with the electronegativity differences, the calculations confirm the higher ionicity of the fluorine (compared to the chlorine) compounds and of the aluminum (compared to the boron) ones. In all systems the ionic sp^2 bonding is exercised through the outer valence orbitals $2a_1'$ and $2e'$. In the boron compounds the out-of-plane orbital $1a_2''$ also has considerable bonding character. In order to describe the Cl $2s$ and $2p$ valence dicationic states in the localized core approach we have to take into account one atomic set of localized chlorine core orbitals. The Cl $2s$ and Cl $2p$ orbitals are separated in energy by almost 70 eV, and the three components of the latter are quite similar in energy, although their degeneracy is removed in the molecule. In the reduced C_{2v} symmetry of the localized core approach these $2p$ components belong to the following irreducible representations: $2p_x \rightarrow b_2$, $2p_y \rightarrow a_1$, and $2p_z \rightarrow b_1$.

In light of the discussion of valence-hole localization in Sec. III, the grouping of the Cl $2s$ and $2p$ valence dicationic states of BCl_3 and $AlCl_3$ illustrated in Fig. 2 is immediately understood. Because of the large energy separation between Cl $2p$ and Cl $2s$ holes we find two distinct energy regions A–D and E–H, containing the Cl $2p$ and Cl $2s$ valence dicationic states, respectively. In both regions the same grouping of states takes place as found in the fluorine spectra, i.e., the first (last) two peaks in both regions refer to outer (inner)

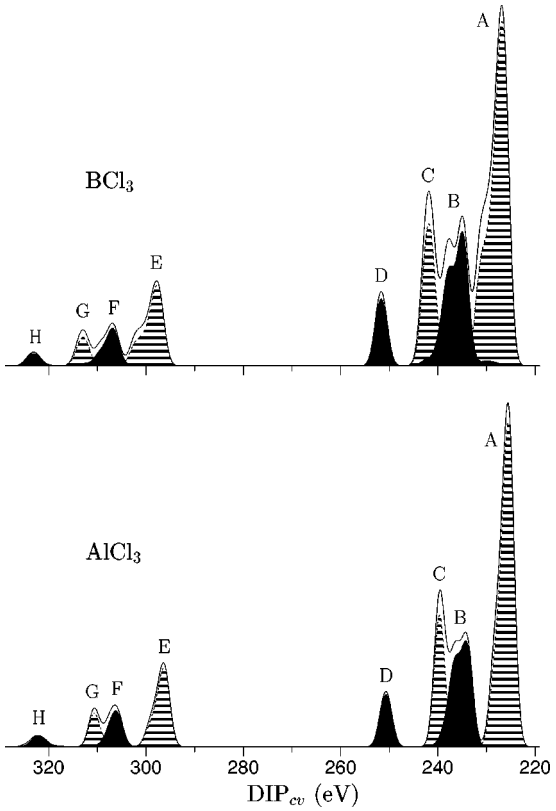

FIG. 2. Full curves represent the Gaussian convolution (FWHM 1.5 eV) of the total ADC $2h$ weight of the Cl $2s$ and $2p$ valence dicationic states of BCl_3 and $AlCl_3$. The striped areas visualize the off-core site Cl component and the full areas reflect the on-core site Cl* component of the $2h$ weight. The remaining area is due to the off-core site central atom component. 509/459 individual states with a $2h$ weight larger than 0.01 contribute to the $BCl_3/AlCl_3$ spectrum. Their energy, $2h$ composition, and $2h$ population can be obtained upon request.

valence holes with alternating off-core and on-core site localization. The extent of valence-hole localization is again clearly demonstrated by the striped and full areas in Fig. 2 which reflect the off-core site Cl and on-core site Cl* component of the $2h$ population, respectively. A numerical measure of the extent of valence-hole localization in the various groups of dicationic states is given by the average $2h$ populations in Table VI. The alternating contribution of the Cl or Cl* component to the $2h$ population varies between 80% and 90% for BCl_3, and between 88% and 94% for $AlCl_3$. In the latter system, localization is stronger because of higher ionicity. In the following we discuss the individual groups in the chlorine spectra in more detail, focusing especially on the differences with the fluorine compounds and on some relevant aspects, like $2h$ configuration mixing, singlet-triplet splittings, and breakdown effects, which cannot be extracted from Fig. 2 and the data in Table VI.

At the onset of the chlorine spectra we encounter the Cl $2p$ outer valence states, separated in the off-core site (group A) and the on-core site (group B). Both groups consist exclusively of dicationic main states, the number of which follows from simple counting arguments: the three Cartesian components of the Cl $2p$ orbital which carries the core-hole, together with the nine outer valence orbitals give rise to 27 singlet-triplet pairs of main states, 18 of the off-core site type in group A and nine of the on-core site type in group B, according to the ratio of 2:1 of the atoms Cl:Cl*. The states in group A behave very much like the corresponding ones in the fluorine spectra, and have an identical charge localization pattern. Although possible in principle, a mixing of different Cl $2p$ Cartesian components does not take place. One notices that, as a result of the more ionic character of $AlCl_3$, its outer valence orbitals cover a smaller energy range and, hence, peak A in the $AlCl_3$ spectrum is narrower than that of BCl_3. The highest lying state of group A and the lowest lying state of group B are separated by a gap of 4.8 eV for $AlCl_3$ and 2.4 eV for BCl_3. It should be noted that these values are much smaller than the corresponding separations between outer valence off-core and on-core site states in AlF_3 (14.8 eV) and BF_3 (11.7 eV).

While the splitting of peak B in the fluorine spectra separates exactly triplet (B_1) from singlet (B_2) states, with each singlet-triplet pair being systematically about $\sim$3.2 eV apart, we find more complex conditions in the chlorine spectra. Here the singlet-triplet splitting varies strongly and the visibly composite structure B in Fig. 2 cannot be separated into one triplet part and one singlet part: the singlet and triplet groups overlap. This finding can be partly explained in terms of the relative orientation of the two holes in the various

TABLE VI. Average two-hole population and variance in percent of the total $2h$ weight for the eight groups of Cl $2s$ and $2p$ valence dicationic states of BCl_3 and $AlCl_3$. The labeling of the peaks refers to Figs. 2 and 3.

	BCl_3			$AlCl_3$		
Peak	Cl*	Cl	B	Cl*	Cl	Al
A	1.27±1.32	88.86±9.85	9.87±8.72	0.20±0.36	91.36±6.74	8.43±6.43
B	83.00±10.93	4.68±3.58	12.33±7.67	89.37±6.67	1.30±1.94	9.33±5.25
C	3.72±2.51	81.48±5.56	14.80±3.21	1.41±1.83	90.22±3.47	8.37±1.83
D	89.66±2.73	1.46±2.09	8.89±1.66	94.19±1.26	0.05±0.19	5.76±1.28
E	2.46±2.76	87.83±9.91	9.71±8.43	1.60±3.17	89.38±7.28	9.02±6.51
F	80.48±12.12	6.38±4.90	13.13±8.64	88.27±8.78	2.62±3.43	9.11±6.55
G	4.56±3.93	81.65±6.67	13.78±4.10	2.14±2.32	88.80±3.75	9.06±2.47
H	89.02±3.78	2.67±3.62	8.31±0.88	93.66±1.54	0.25±0.28	6.09±1.44

TABLE VII. Double-ionization potential (DIP_{cv}) and two-hole atomic population analysis of the outer valence on-core site Cl $2p$ valence dicationic states of $AlCl_3$ (group *B* in Table VI and Fig. 2). All relevant contributions to the chlorine on-core site (Cl*) population are reported.

			Cl* population						total
$2h$ character	State	DIP_{cv} (eV)	p_x^{-2}	p_y^{-2}	p_z^{-2}	$p_x^{-1}p_y^{-1}$	$p_x^{-1}p_z^{-1}$	$p_y^{-1}p_z^{-1}$	$2h$ weight
$2p_x3p_z/2p_z3p_x$	$^1A_2$	233.1911					0.7083		0.7452
$2p_x3p_x/2p_z3p_z$	$^3A_1$	233.7324	0.3668	0.0000	0.3427				0.7456
$2p_x3p_z/2p_z3p_x$	$^3A_2$	233.7326					0.7095		0.7456
$2p_y3p_x$	$^1B_2$	233.9658				0.6704			0.7448
$2p_y3p_z$	$^1B_1$	233.9729						0.6684	0.7458
$2p_x3p_x/2p_z3p_z$	$^3A_1$	234.1273	0.3336	0.0167	0.3547				0.7458
$2p_y3p_x$	$^3B_2$	234.2468				0.6961			0.7445
$2p_y3p_z$	$^3B_1$	234.2544						0.6935	0.7458
$2p_x3p_z/2p_z3p_x$	$^3A_2$	235.0276					0.7106		0.7457
$2p_y3p_y$	$^3A_1$	235.8624	0.0105	0.5478	0.0106				0.7445
$2p_x3p_y$	$^3B_2$	236.3078				0.5802			0.7450
$2p_z3p_y$	$^3B_1$	236.3107						0.5797	0.7451
$2p_x3p_z/2p_z3p_x$	$^1A_2$	236.3226					0.7138		0.7487
$2p_x3p_x/2p_z3p_z$	$^1A_1$	236.3226	0.3591	0.0000	0.3547				0.7487
$2p_x3p_x/2p_z3p_z$	$^1A_1$	237.0231	0.2790	0.1218	0.2814				0.7492
$2p_x3p_y$	$^1B_2$	237.3203				0.6037			0.7479
$2p_z3p_y$	$^1B_1$	237.3212						0.6034	0.7485
$2p_y3p_y$	$^1A_1$	238.7149	0.0736	0.4182	0.0748				0.7503

states of group *B*, comprising essentially all possible combinations of one $2p$ hole and one outer valence (i.e., $3p$) hole in the Cl* atom. The two-hole population analysis helps us to clarify this situation, as shown in Table VII. The table reports, for the states of group *B* of $AlCl_3$, the schematic $2h$ composition and a detailed analysis of the Cl* population (the dominant character). Because of the $2p$ character of the core hole and the $3p$ character of the valence hole, only the *p* Cartesian components of the Cl* population are shown. As expected, group *B* comprises 18 main states, nine of each spin multiplicity. The corresponding results for BCl_3 are similar. While inspecting the table it is useful to bear in mind that the *y* Cartesian direction corresponds to the C_2 rotation axis of Cl^*AlCl_2, while the molecule lies in the *xy* plane. What emerges from the table is that the states of A_1 symmetry display a parallel orientation of the Cl $2p$ and $3p$ holes, which are instead perpendicularly oriented in all other states. Because of this, the A_1 states show a substantial singlet-triplet splitting of 2.5–3 eV, while the splitting is much smaller for the perpendicular orientation of the holes. In the latter situation we find singlet-triplet splittings of about -0.5 eV at lower energy (i.e., the singlet state lies below the corresponding triplet) and about 1 eV at higher energy.

One noteworthy result also shown in Table VII is the mixing of $2h$ Cartesian components in the A_1 and A_2 states leading to a spatial reorientation of the $2p$ core hole in the dicationic states. In the A_1 states the localized $2h$ configurations with parallel holes ($2p_x3p_x$) and ($2p_z3p_z$) couple, resulting in an orientation of the Cl $2p$ and $3p$ holes which is not along but between the Cartesian axes. A similar coupling takes place between the localized $2h$ configurations ($2p_x3p_z$) and ($2p_z3p_x$) in the A_2 states, leading to an orientation of the two holes (perpendicular to each other) between the Cartesian *x* and *z* axes.

Owing to considerable breakdown effects of the MO picture starting among the Cl $2p$ inner valence off-core site states, a conclusive analysis of the states in group *C* and in the subsequent groups of the chlorine spectra becomes difficult. A higher-order method should be used to accurately compute the states in these energy ranges, where the MO picture of ionization is generally inapplicable (see Sec. III C). For the Cl $2p$ inner valence on-core site states the breakdown is already so strong that no state reaches a $2h$ weight of 0.4. It is conspicuous that the large singlet-triplet separation which has been found for the F $1s$ inner valence on-core site states shown in Fig. 1 (6 eV), is not observed for the states in group *D* of the chlorine spectra. Apart from the breakdown effects taking place in the latter, this is due to the weaker interaction of the Cl $2p$ and $3s$ holes compared to F $1s$ and $2s$ holes. As a result, the singlet-triplet splittings of the on-core site states of group *D* in the chlorine spectra are as small as typically found for the off-core site states in group *C*.

The states in groups *E*–*H* at the high-energy side of the chlorine spectra are Cl $2s$ valence dicationic states. With respect to the on or off-site localization of the valence hole, as well as to its outer or inner valence character, the states lie in the same sequence as the Cl $2p$ valence dicationic states of groups *A*–*D*. The average $2h$ populations in Table VI evidence the similar distribution of the valence hole for corresponding Cl $2p$ and Cl $2s$ valence dicationic states. In the Cl $2s$ valence dicationic states we encounter a complete breakdown of the MO picture of ionization: the $2h$ weight of any state is smaller than 0.24 in the case of BCl_3, and does not reach 0.32 in the case $AlCl_3$. Therefore, we shall not

pursue the analysis of this complex manifold of states further.

B. *KLV* Auger spectra

Because of the multitude of core-valence dicationic states, which are at the origin of the *KLV* Auger spectra of even relatively simple polyatomic molecules such as the D_{3h} systems studied here, it seems practically impossible to calculate accurate individual transition rates for these hundreds or thousands of states. But the analysis of the correlated wave function in terms of localization of the two holes in the final dicationic states (as outlined in Sec. III B) provides us with the key not only to interpret and understand these complex spectra but also to theoretically predict with reasonable confidence the spectral line shapes.

Since the Auger decay is essentially an intra-atomic process, the Auger intensities reflect the local two-hole density in the dicationic states around the atomic site where the primary (deep) core vacancy has been created. It is therefore clear that only states with a significant component of the $2h$ density located at a given atom, can have an appreciable rate of decay from the corresponding core-hole state. In this sense, the Auger process is site selective. We can further expect to observe a qualitative correspondence between the energy distribution of the one-site contribution of a given atom to the $2h$ weight and the energy distribution of the Auger spectral intensity originating from core ionization of that atom. This correspondence has indeed been shown to hold with remarkable precision in the case of the commonly investigated valence-type (CVV) Auger spectra [20,23–25].

Our arguments appear particularly appropriate for the chlorine *KLV* Auger spectra of ionic molecules like BCl_3 and $AlCl_3$. The site selectivity of the Auger process requires that the secondary (L-shell) core vacancy is localized on the same atom where the primary (K-shell) core-hole has been created and that only the on-core site component of the $2h$ weight contributes to the Auger intensity. Because of the pronounced on-core or off-core site localization of the valence hole in each of the eight groups A–H of Cl $2s$ and $2p$ valence dicationic states, these groups must either appear in the chlorine spectra (on-core site) or have almost zero intensity (off-core site). According to the Cl $2p$ outer valence, Cl $2p$ inner valence, Cl $2s$ outer valence, and Cl $2s$ inner valence grouping of the states, one expects a simple Auger spectrum consisting of the four groups of on-core site states, which are labeled *B*, *D*, *F*, and *H* in Fig. 2, whereas the states in groups *A*, *C*, *E*, and *G* carry very little intensity and virtually disappear from the chlorine spectra.

In Fig. 3 our arguments are illustrated by the theoretical chlorine *KLV* Auger spectra of BCl_3 and $AlCl_3$ which have been obtained from Gaussian convolution of the on-core site (Cl*) population of the Cl $2s$ and $2p$ valence dicationic states. The interpretation of the spectra in the light of the $2h$ density analysis clarifies some relevant and general questions. Their simple atomiclike appearance emerges as a result of the very pronounced valence-hole localization taking place in the dense manifold of dicationic states. Because of the intra-atomic nature of the Auger process, this phenomenon enforces *extremely strict selection rules* on the decay transition rates, whereby all the states with off-core site character are not populated at all. This fact deprives the ligand *KLV* Auger spectra of the present and other ionic molecules with strongly electronegative constituents of all relevant information about the molecular environment, reducing these spectra to an indistinct self-image of the ligand atom itself. This is obvious, for example, in Fig. 3, where the chlorine spectra of BCl_3 and $AlCl_3$ are very similar to each other. This self-imaging atomic picture is a common interpretive key in Auger spectroscopy. As has been pointed out [25,46] it is, however, completely inapplicable to the central atom Auger spectra of systems like the ones studied here: in this case, a complementary *foreign-imaging* character of the spectra emerges instead, yielding a distinct, fingerprinting image of the molecular environment. The applicability of the foreign-imaging picture for the central atom *KLV* Auger spectrum will be studied in Sec. VI B for the aluminum compounds AlF_3 and $AlCl_3$.

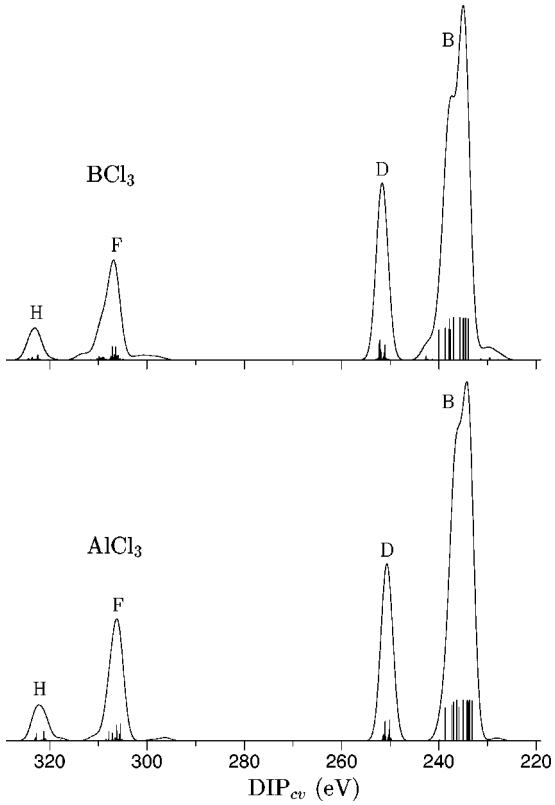

FIG. 3. Theoretical chlorine *KLV* Auger spectrum of BCl_3 and $AlCl_3$. The theoretical spectrum is obtained by Gaussian convolution (FWHM 1.5 eV) of the on-core site Cl* component of the total ADC $2h$ weight. The contribution of each individual state is shown as a vertical bar.

Here we would like to point out one useful practical difference in the interpretation CVV and *KLV* spectra. In the former, the manifold of final valence-valence dicationic states is correctly thought to be the same in both the ligand and central atom spectra, spanning the same energy range, and the different intensity of the states can then be roughly related to their different one-site $2h$ population. In the *KLV* spectra, on the other hand, the strong *a priori* atomic localization of the L-shell final hole can already be thought as if preliminarily *selecting* a specific submanifold of final core-valence dicationic states, lying in a specific energy range,

namely, those states where the *L*-shell hole is located at the same atomic site of the primary *K*-shell vacancy. The intensity of the states can then simply be put in qualitative relation to their on-core site population.

V. B 1*s* VALENCE DICATIONIC STATES OF BF_3 AND BCl_3

Before we discuss the B 1*s* valence dicationic states of BF_3 and BCl_3, two general aspects are to be emphasized concerning the core-valence dicationic states of D_{3h} molecules MX_3 when the core hole is localized on the central atom. First, the system M^*X_3—the molecule with one central atom core hole—maintains the D_{3h} symmetry of MX_3. The three ligands are symmetry equivalent, and the total $2h$ weight of the dicationic states can be separated into the on-core site contribution M^* and one off-core site contribution *X*. Second, throughout the ligand atom spectra we encountered strong valence-hole localization effects via $2h$ configuration mixing in order to minimize the hole-hole repulsion in the off-core site states. In the central atom spectra the dicationic states have automatically a leading off-core site character, since all valence electrons are predominantly localized on the electronegative ligands. Consequently, there is no *a priori* obvious reason for a spatial rearrangement of the valence hole. Indeed, we do not find considerable $2h$ mixing throughout *all* central atom spectra.

The results of the ADC calculations on the B 1*s* valence dicationic states of BF_3 and BCl_3 are depicted in Fig. 4. The dominating off-core site character of all the states is clearly shown by the tiny on-core site B* component (full areas): For BF_3 and BCl_3 the computed average B* percent population in the A_1 group of states are 3% and 2%, respectively. These values increase somewhat in the other groups, reaching a maximum of about 18% for the A_2 group of BCl_3. The division of the boron spectra in two regions *A* and *B*, as well as the size of the energy gap between them, is simply due to the energy difference between the outer and inner valence orbitals which amounts to 21.4 eV for BF_3 and 11.3 eV for BCl_3, respectively. While the outer valence states in group *A* are all main states, we encounter strong breakdown effects among the inner valence states in group *B*. In the case of BF_3 few weak shake-up satellites, which derive from the out-of-plane orbitals $1a_2''$ and $1e''$, appear around 247 eV, before the inner valence breakdown region starts at 252 eV. The situation is somewhat different in the case of BCl_3. We find various weak shake-up satellites in the narrow region between the outer valence main states, which cease at 228 eV, and the inner valence breakdown states starting at 235 eV.

Owing to their main state character, the B 1*s* outer valence dicationic states in group *A* can be interpreted in the MO picture of ionization. The absence of an appreciable $2h$ configuration mixing in these states entails a clear one-to-one correspondence between the states and the HF outer valence orbitals. As a consequence, their Mulliken population analysis yields directly the valence-hole distribution in the dicationic states. Group A_1 of the boron spectra is made up of five singlet-triplet pairs which derive from the outermost valence orbitals $1a_2'$, $1e''$, and $3e'$. Their halogen nonbonding character leads to the mentioned small B* population and to slightly *negative* singlet-triplet splittings (triplet states are preceded by their singlet counterparts) of about -0.1 eV. The highest lying state ($^3E'$) in group A_1 is separated from the lowest lying state ($^3A_2''$) in group A_2 by about 2.5 eV. The four singlet-triplet pairs in group A_2 derive from the increasingly bonding orbitals $1a_2''$, $2e'$, and $2a_1'$. This explains the marked B* population for these states and the larger positive singlet-triplet splittings: these splittings are about 0.4 eV for states originating from $1a_2''$ or $2e'$ and 1.1–1.3 eV for states resulting from the $2a_1'$ orbital.

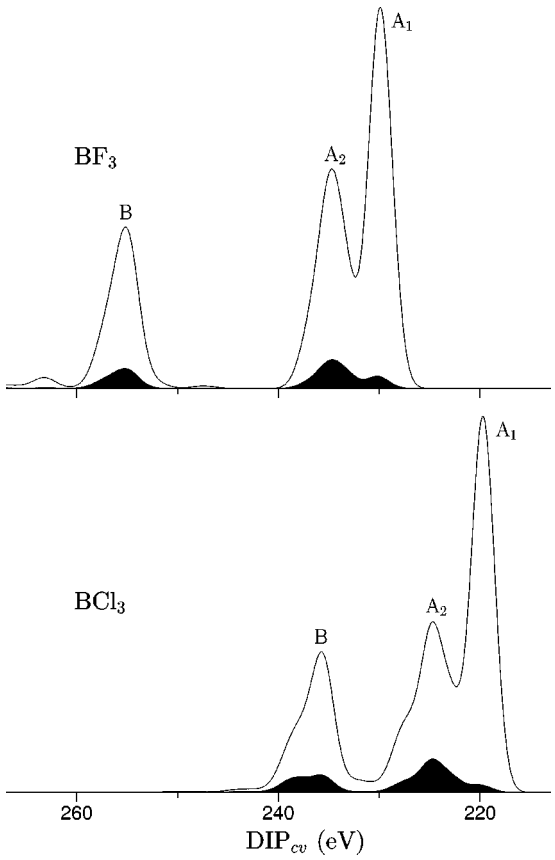

FIG. 4. The full curves represent the Gaussian convolution (FWHM 1.5 eV) of the total ADC $2h$ weight of the B 1*s* valence dicationic states of BF_3 and BCl_3. The full areas visualize the on-core site B* component of the $2h$ weight. The remaining area is due to the off-core site ligand atom component. 82/92 individual states with a $2h$ weight larger than 0.01 contribute to the BF_3/BCl_3 spectrum. Their energy, $2h$ composition, and $2h$ population can be obtained upon request.

VI. Al 2*s* AND 2*p* VALENCE DICATIONIC STATES OF AlF_3 AND $AlCl_3$

A. Results and analysis

The results of the ADC calculations on the Al 2*s* and 2*p* valence dicationic states of AlF_3 and $AlCl_3$ are illustrated in Fig. 5. Because of the energy gap of more than 45 eV between the Al 2*p* and Al 2*s* orbitals computed at the HF level, the Al 2*p* valence dicationic states in groups *A* and *B* are well separated from the Al 2*s* valence dicationic states in groups *C* and *D*. The states in groups *A* and *C* derive from the outer valence orbitals, and those in groups *B* and *D* from

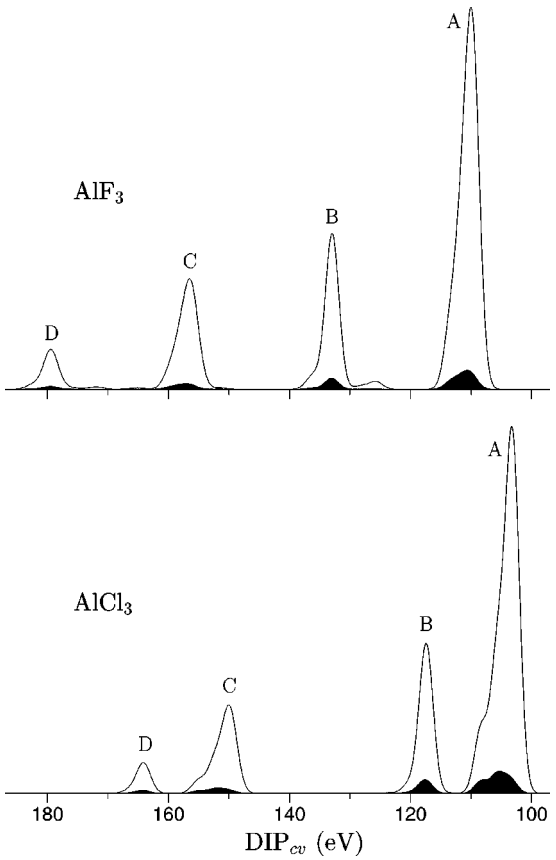

FIG. 5. The full curves represent the Gaussian convolution (FWHM 1.5 eV) of the total ADC $2h$ weight of the Al $2s$ and $2p$ valence dicationic states of AlF_3 and $AlCl_3$. The full areas visualize the on-core site Al* component of the $2h$ weight. The remaining area is due to the off-core site ligand atom component. 596/621 individual states with a $2h$ weight larger than 0.01 contribute to the $AlF_3/AlCl_3$ spectrum. Their energy, $2h$ composition, and $2h$ population can be obtained upon request.

the inner valence orbitals. The gap between peaks *A* and *B* as well as between peaks *C* and *D* is much smaller in the $AlCl_3$ spectrum than in the AlF_3 spectrum. As in the boron spectra this is simply due to the very different separation between the inner and outer valence orbitals, which is 22.7 eV for AlF_3 and 13.0 eV for $AlCl_3$. While the Al $2p$ outer valence states in group *A* are all main states, we encounter strong correlation effects among the inner valence states in group *B*, and a complete breakdown of the MO picture for the Al $2s$ states in groups *C* and *D*. In the AlF_3 spectrum some weak satellite states gather between 125 and 129 eV, giving rise to the weak structure in Fig. 5 at the low-energy side of peak *B*. In the $AlCl_3$ spectrum no satellites are found between the individual groups.

Like the boron states, the aluminum states also have the valence hole predominantly localized on the ligand atoms, i.e., they are predominantly off-core site states. In fact, owing to the higher ionicity of the aluminum compounds, their off-core site character is generally even more pronounced than that of the boron states: The average percent Al* population does not exceed 10% in any group of states, being always somewhat higher in the inner-valence groups *B* and *D*.

The absence of an appreciable $2h$ configuration mixing throughout the aluminum spectra permits an interpretation of the main states in group *A* in terms of HF orbitals. We have mentioned how, in the boron spectra, the energy gap between the five nonbonding outermost ($1a_2'$, $1e''$, and $3e'$) and the four innermost outer valence orbitals ($1a_2''$, $2e'$, and $2a_1'$) leads to the splitting of peak *A*. In contrast to this, the corresponding orbitals of the aluminum compounds cannot be clearly separated into nonbonding and bonding ones, their bonding character continuously growing with increasing energy. This explains the narrower peak *A* in the aluminum spectra. In the case of $AlCl_3$, however, the innermost outer valence orbital $2a_1'$ is still separated from $2e'$ by 2.0 eV and, thus, $2a_1'$ ionization is responsible for the shoulders at the high energy side of peaks *A* and *C*.

In line with the small *on-core site* Al* population of the dicationic states of AlF_3 and $AlCl_3$, we do not find considerable singlet-triplet splittings among the main states in group *A*. Of course, the actual values depend not only on the size of the Al* population but also on the spatial arrangement of the outer valence hole relative to the Cartesian Al $2p$ component. The splittings of singlet-triplet pairs that derive from the five outermost valence orbitals are nearly zero (-0.05–0.0 eV), while the four innermost outer valence orbitals give rise to splittings from -0.4 to 0.6 eV. In general, splittings of few tenths of an eV are observed when the dicationic states have vacancies oriented in the same plane, i.e., when one in-plane (out-of-plane) outer valence orbital is interacting with an Al $2p_{x,y}$ (Al $2p_z$) component.

B. *KLV* Auger spectra

By following the same lines of analysis as in Sec. IV B, the appearance of the theoretical aluminum *KLV* Auger spectra of AlF_3 and $AlCl_3$ in Fig. 6 is of immediate interpretation. The Auger process is here probing the $2h$ density at the aluminum site in a situation where, as we have seen, all states have a dominating off-core site character and their relatively small on-core site Al* population is quite uniformly distributed over the entire spectrum. The absence of an alternating off-core and on-core site character of the states obviously prevents the occurrence of any *a priori* strong selection rule similar to that found for the Cl *KLV* spectra. We conclude that a simple four-peaked spectral structure according to the Cl $2p$ outer valence, Cl $2p$ inner valence, Cl $2s$ outer valence, and Cl $2s$ inner valence groupings of the states should be expected in the Al *KLV* spectra, each of the four well-separated groups producing one distinct band. Despite the quite uniform distribution of the Al* population over the entire spectrum of dicationic states, there are two obvious differences between the total $2h$ density curve in Fig. 5 and the on-core site $2h$ density curve in Fig. 6, the latter being related to the Al *KLV* Auger spectrum. First, as mentioned above, the relatively higher Al* population of the inner-valence states translates into a stronger relative intensity of peaks *B* and *D* in the Auger spectra. Second, in the case of $AlCl_3$ the shoulder at the high-energy side of peaks *A* and *C* is more pronounced in the Auger spectrum than in Fig. 5 because the innermost outer valence orbital $2a_1'$ is definitely the most bonding orbital of $AlCl_3$.

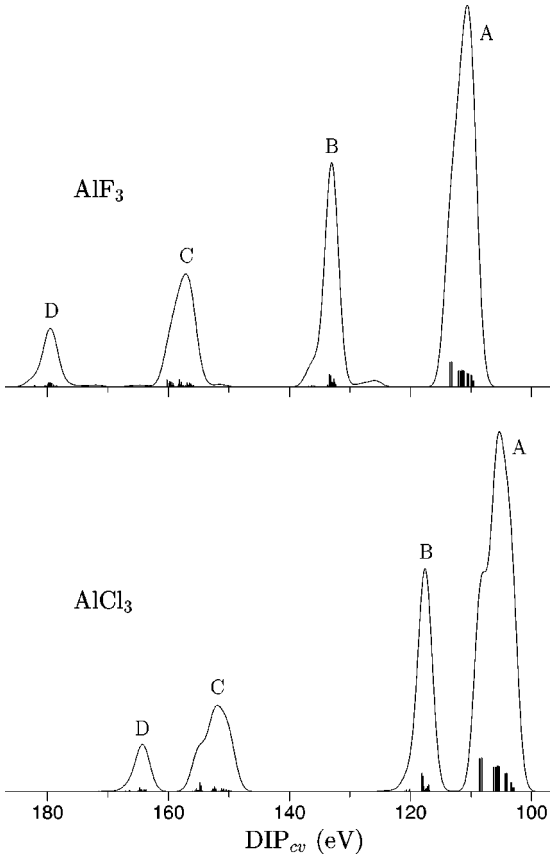

FIG. 6. Theoretical aluminum *KLV* Auger spectrum of AlF_3 and $AlCl_3$. The theoretical spectrum is obtained by Gaussian convolution (FWHM 1.5 eV) of the on-core site Al* component of the total ADC $2h$ weight. The contribution of each individual state is shown as a vertical bar.

The conceptual differences between the results of Auger decay from the Cl $1s$ and Al $1s$ vacancies stand out very evidently from our analysis. While the ligand atom spectrum is strictly atomic in appearance, bearing hardly any trace of the chemical environment, exactly the opposite is true for the central atom spectrum. Here all the atomic information is lost and the spectrum reflects the energy distribution of the dicationic states which is exclusively determined by the surrounding molecular environment where the valence vacancies are produced. This characteristic of the central atom spectrum has been defined foreign imaging in the CVV Auger spectroscopy of ionic molecules [25,46]. The final dicationic states resulting from the CVV Auger process hardly exhibit valence vacancies on the atom with the primary core vacancy. In contrast, the *KLV* Auger decay populates heterogeneous dicationic states, where one vacancy, the *L*-shell vacancy, is on the atom with the primary *K*-shell vacancy. Nevertheless, the foreign imaging picture is appropriate to interpret the central atom *KLV* Auger spectra of highly ionic molecules, like the systems studied here, since the second vacancy is essentially located on the ligands. The ''foreign image,'' or complete lack of atomic character, in these Auger spectra is of course a direct consequence of the intra-atomic nature of the decay process. The aluminum atom undergoes a pronounced electron loss in the valence shell upon binding three fluorine or chlorine atoms, and therefore the valence hole cannot appreciably localize at the Al site. Since all available final states have the valence hole created away from the Al atom, all are populated with roughly comparable decay rates and the resulting Al *KLV* spectrum is utterly unrelated to the corresponding one of the isolated atom.

VII. CONCLUSIONS

A. Hole localization effects in core-valence dicationic states

In the present work we have investigated theoretically core-valence double vacancies in ionic molecules containing strongly electronegative, symmetry equivalent ligands. As explicit examples we have studied the core-valence doubly ionized states of BF_3, AlF_3, BCl_3, and $AlCl_3$ using two-particle Green's-function methods. Two classes of core-valence dicationic states derive from these molecules: In the first class the core vacancy is localized on the ligand atom, while in the second class the central atom carries the core hole. The manifold of correlated dicationic states in the core-valence double-ionization spectra of the above molecules was analyzed by studying their two-hole ($2h$) density distribution. It is found that in *all* states of the first class the valence hole is also strongly localized on one ligand atom, naturally giving rise to two types of states: on-core site states, where the valence hole is on the same atom carrying the core hole; and off-core site states, where the valence vacancy is on another ligand atom. This on-core or off-core site localization of the valence hole, together with its inner or outer valence character, dictates, via hole-hole repulsion, the energy distribution of the states, which come in dense and well-separated groups. The valence-hole density at the central atom is much smaller and quite uniformly distributed over all these groups. Apart from symmetry considerations, the on-core site population is the relevant quantity to estimate the strength of the hole-hole interaction in the dicationic states. This is revealed by the alternating off-core and on-core site character of the individual groups as well as by the energy splitting of singlet-triplet pairs of main states which is quasinegligible in the off-core site states and may reach several eV in the on-core site states. The valence-hole localization on the ligands is realized by a strong coupling of $2h$ configurations in the dicationic states involving the delocalized ground-state valence orbitals. While only this kind of $2h$ mixing is possible in the F $1s$ and Cl $2s$ valence dicationic states, the spatial reorganization of a localized Cl $2p$ hole also becomes feasible by the mixing of $2h$ configurations with different Cl $2p$ Cartesian components. However, this specific kind of $2h$ mixing, involving core and valence orbitals, is operating solely among some of the Cl $2p$ outer valence on-core site states, because here the hole-hole repulsion can be strong and markedly depends on the Cl $2p$ Cartesian component interacting with the nonspheric Cl $3p$ distribution of the outer valence hole.

A very different picture describes in general the dicationic states of the second class—those with a central atom core hole. In all systems studied here, we have found that each one of these states essentially derives from one specific delocalized ground-state valence orbital: In complete contrast to the ligand core hole states of the first class, there are no hole localization effects via $2h$ configuration mixing. This finding can be understood by the fact that the central atom undergoes a pronounced electron loss in the valence shell

upon binding three electronegative ligands. As a consequence, the dicationic states of the second class have automatically a leading off-core site character and there is no physical reason for a spatial reorganization of the valence hole (other than small higher order correlation effects). Indeed, the weak hole-hole interaction in these states is reflected by the small or moderate singlet-triplet splitting of the B $1s$ and Al $2p$ outer valence main states.

The strength of valence-hole localization in both types of dicationic states, with a ligand or central atom core vacancy, is related to the ionicity of the molecular system. This means that the strongest valence hole localization effects are found for AlF_3 and the weakest for BCl_3. For example, about 94% of the valence-hole density is localized at one fluorine atom in the dicationic states of AlF_3. Of course, the ionic molecules studied here are extreme examples of this situation and a continuous wide range of interesting *weaker* cases exists. $2h$ localization effects at the ligand atoms of ionic molecules are already known from the valence double ionization of fluorine compounds like BF_3 and SiF_4 [20,25]. These effects are even more pronounced in the core-valence dicationic states.

B. Ligand and central atom *KLV* Auger spectra in the light of foreign imaging

By analogy to the usual Auger decay leading to valence doubly ionized states, an initial deep core-hole state may decay into core-valence dicationic states by emission of a further electron, when the primary core hole is localized on an atom which contains at least one more energetically higher core shell. In $AlCl_3$, for example, an initial Cl $1s$ or Al $1s$ vacancy may decay to the Cl $2s$ and $2p$ or Al $2s$ and $2p$ valence dicationic states discussed here. The $2h$ population analysis can be used to simulate the resulting KLV Auger spectra. The intra-atomic nature of the Auger decay requires that the L-shell core vacancy be localized on the same atom where the K-shell hole has been created and that only the on-core site component of the total $2h$ density contribute to the Auger intensity. Thus very strict selection rules are imposed in the chlorine spectrum, almost perfectly segregating the on-core site states from the off-core site states. According to their respective character, the states cluster in energy giving rise to well separated groups. Therefore, either a peak (group of states) appears in the spectrum because of the on-core site character of its component states, or it has essentially zero intensity. As a result, apart from typical, molecule-dependent, overall shifts, the ligand spectrum is strictly atomiclike and contains almost no information about the molecular system, reducing this spectrum to an indistinct self-image of the ligand atom itself.

On the other hand, the entire information concerning the molecular system, which is so effectively filtered out of the ligand spectrum, is fully recovered in the central atom (aluminum) spectrum. The latter, because of the dominant valence-hole localization at the ligands, loses all atomic information and yields instead a complete and detailed image of the surrounding molecular environment where the valence vacancies are located. This foreign imaging spectrum is essentially shaped by the relatively small valence-hole density at the central core-hole atom which is quite uniformly distributed over the entire spectrum. Hence no strict selection rules are enforced and the surrounding chemical environment leaves its fingerprints on the spectrum.

The foreign imaging picture has already been proposed for the central atom CVV Auger spectroscopy of ionic molecules, where it yields a very satisfactory reproduction and interpretation of experimental results [20,25,46]. More structured and complex ligand and central atom CVV [25] and KLV Auger spectra can be expected for less ionic molecules. In all these cases, the results and the concepts illustrated in the present work may serve as a useful guideline for analysis.

ACKNOWLEDGMENT

Financial support by the Deutsche Forschungsgemeinschaft is gratefully acknowledged.

[1] M. Thompson, M. D. Baker, A. Christie, and J. F. Tyson, *Auger Electron Spectroscopy* (Wiley, New York, 1985).
[2] P.G. Fournier, J. Fournier, F. Salama, D. Stärk, S.D. Peyerimhoff, and J.H.D. Eland, Phys. Rev. A **34**, 1657 (1986).
[3] R. Cooks, T. Ast, and J. Beynon, Int. J. Mass Spectrom. Ion Phys. **11**, 490 (1973).
[4] D. Mathur and C. Badrinathan, J. Phys. B **20**, 1517 (1987), and references therein.
[5] G. Dujardin, L. Hellner, D. Winkoun, and M.J. Besnard, Chem. Phys. **105**, 291 (1986).
[6] P. Lablanquie, J.H.D. Eland, I. Nenner, P. Morin, J. Delwiche, and M.-J. Hubin-Franskin, Phys. Rev. Lett. **58**, 992 (1987).
[7] J.H.D. Eland, S.D. Price, J.C. Cheney, P. Lablanquie, I. Nenner, and P.G. Fournier, Philos. Trans. R. Soc. London, Ser. A **324**, 247 (1988).
[8] P. Lablanquie, J. Delwiche, M.-J. Hubin-Franskin, I. Nenner, P. Morin, K. Ito, J.H.D. Eland, J.-M. Robbe, G. Gandara, J. Fournier, and P.G. Fournier, Phys. Rev. A **40**, 5673 (1989).
[9] L.S. Cederbaum, F. Tarantelli, A. Sgamellotti, and J. Schirmer, J. Chem. Phys. **85**, 6513 (1986); **86**, 2168 (1987).
[10] S. Bodeur, P. Millié, E. Lizon à Lugrin, I. Nenner, A. Filipponi, F. Boscherini, and S. Mobilio, Phys. Rev. A **39**, 5075 (1989).
[11] J.L. Ferrer, S. Bodeur, and I. Nenner, J. Electron Spectrosc. Relat. Phenom. **52**, 711 (1990).
[12] E.M.L. Ohrendorf, L.S. Cederbaum, and F. Tarantelli, Phys. Rev. A **44**, 205 (1991); Chem. Phys. Lett. **183**, 1 (1991).
[13] D.A. Lapiano-Smith, C.I. Ma, K.T. Wu, and D.M. Hanson, J. Chem. Phys. **90**, 2162 (1989).
[14] A. Cesar, H. Ågren, A. Naves de Brito, S. Svensson, L. Karlsson, M.P. Keane, B. Wannberg, P. Baltzer, P.G. Fournier, and J. Fournier, J. Chem. Phys. **93**, 918 (1990).
[15] D.E. Ramaker, Crit. Rev. Solid State Mater. Sci. **17**, 211 (1991).
[16] S. Svensson and L. Karlsson, Phys. Scr. **T41**, 132 (1992).
[17] C.-M. Liegener, Chem. Phys. **92**, 97 (1985).

[18] F.P. Larkins, J. Electron Spectrosc. Relat. Phenom. **51**, 115 (1990).
[19] R.L. Graham and D.L. Yeager, J. Chem. Phys. **94**, 2884 (1991).
[20] F. Tarantelli, A. Sgamellotti, and L.S. Cederbaum, J. Chem. Phys. **94**, 523 (1991).
[21] H. Ågren, A. Cesar, and C.-M. Liegener, Adv. Quantum Chem. **23**, 1 (1992).
[22] F.P. Larkins, J. McColl, and E.Z. Chelkowska, J. Electron Spectrosc. Relat. Phenom. **67**, 275 (1994).
[23] D. Minelli, F. Tarantelli, A. Sgamellotti, and L.S. Cederbaum, J. Chem. Phys. **99**, 6688 (1993); J. Electron Spectrosc. Relat. Phenom. **74**, 1 (1995).
[24] F. Tarantelli, L.S. Cederbaum, and A. Sgamellotti, J. Electron Spectrosc. Relat. Phenom. **76**, 47 (1995), and references therein.
[25] F.O. Gottfried, L.S. Cederbaum, and F. Tarantelli, Phys. Rev. A **53**, 2118 (1996); J. Chem. Phys. **104**, 9754 (1996).
[26] H.D. Schulte, L.S. Cederbaum, and F. Tarantelli, J. Chem. Phys. **105**, 11 108 (1996).
[27] F.J. Wuilleumier, L. Journel, B. Rouvellou, D. Cubaynes, J.-M. Bizau, Z. Liu, J. Liu, M. Richter, P. Sladeczek, K. H. Selbman, and P. Zimmermann, Phys. Rev. Lett. **73**, 3074 (1994).
[28] D. Nordfors, A. Nilsson, N. Mårtensson, S. Svensson, U. Gelius, and H. Ågren, J. Electron Spectrosc. Relat. Phenom. **56**, 117 (1991), and references therein.
[29] U. Becker, D. Szostak, M. Kupsch, H.G. Kerkhoff, B. Langerand, and R. Wehlitz, J. Phys. B **22**, 749 (1989).
[30] V. Schmidt, Rep. Prog. Phys. **55**, 1431 (1992), and references therein.
[31] P. Weightman, J. Electron Spectrosc. Relat. Phenom. **68**, 127 (1994).
[32] P.S. Bagus and J.F. Schaefer, J. Chem. Phys. **56**, 224 (1972).
[33] A. Denis, J. Langlet, and J.P. Malrieu, Theor. Chim. Acta **38**, 49 (1975).
[34] L.S. Cederbaum and W. Domcke, J. Chem. Phys. **66**, 5085 (1977).
[35] L.S. Cederbaum, Phys. Rev. A **35**, 622 (1987).
[36] H.D. Schulte and L.S. Cederbaum, J. Chem. Phys. **103**, 698 (1995), and references therein.
[37] J. Schirmer and A. Barth, Z. Phys. A **317**, 267 (1984).
[38] A. Tarantelli and L.S. Cederbaum, Phys. Rev. A **39**, 1656 (1989).
[39] E.M.L. Ohrendorf, H. Köppel, L.S. Cederbaum, F. Tarantelli, and A. Sgamellotti, J. Chem. Phys. **91**, 1734 (1989).
[40] E.M.L. Ohrendorf, F. Tarantelli, and L.S. Cederbaum, J. Chem. Phys. **92**, 2984 (1990).
[41] L.S. Cederbaum, W. Domcke, J. Schirmer, and W. von Niessen, Adv. Chem. Phys. **65**, 115 (1986), and references therein.
[42] H.D. Meyer and S. Pal, J. Chem. Phys. **91**, 6195 (1989).
[43] T.H. Dunning, Jr., J. Chem. Phys. **55**, 716 (1971).
[44] R. Ahlrichs and P.R. Taylor, J. Chem. Phys. **78**, 315 (1981).
[45] *Atomic and Molecular Physics. Structure Data of Free Polyatomic Molecules*, edited by K.-H. Hellwege and O. Madelung, Landolt-Börnstein, New Series, Group II, Vol. 7 (Springer, Berlin, 1976).
[46] F. Tarantelli and L.S. Cederbaum, Phys. Rev. Lett. **71**, 649 (1993).